Histone chaperone HIRA, Promyelocytic Leukemia (PML) protein and p62/SQSTM1 coordinate to regulate inflammation during cell senescence and aging.

Nirmalya Dasgupta[1], Xue Lei[1], Rouven Arnold[1], Marcos Garcia Teneche[1], Karl N. Miller[1], Adarsh Rajesh[1], Andrew Davis[1], Valesca Anschau[2], Alexandre R. Campos[2], Rebecca Gilson[3], Aaron Havas[1], Shanshan Yin[1], Zong Ming Chua[1], Jessica Proulx[1], Michael Alcaraz[1], Mohammed Iqbal Rather[4], Josue Baeza[5], David C. Schultz[6], Shelley L. Berger[7], and Peter D. Adams[1*].

[1]Sanford Burnham Prebys Medical Discovery Institute; 10901 N Torrey Pines Rd, La Jolla, CA 92037, USA.

[2]Proteomics Facility, Sanford Burnham Prebys Medical Discovery Institute; 10901 N Torrey Pines Rd, La Jolla, CA 92037, USA.

[3] Biophotonics Core, Salk Institute for Biological Studies; 10010 N Torrey Pines Rd, La Jolla, CA 92037

[4]Beatson Institute for Cancer Research and University of Glasgow, Garscube Estate, G61 1BD, UK.

[5]Department of Biochemistry and Biophysics, Perelman School of 5Medicine, University of Pennsylvania, Philadelphia, PA 19104, USA.

[6]High Throughput Screening Core, Department of Microbiology, University of Pennsylvania, Philadelphia, PA 19104, USA.

[7]Department of Cell and Developmental Biology, University of Pennsylvania, Philadelphia, PA 19104, USA.

*Corresponding author: padams@sbpdiscovery.org

Abstract

Cellular senescence, a stable proliferation arrest caused by a range of cellular stresses, is a *bona fide* cause of cell and tissue aging. As well as proliferation arrest, cell senescence is associated with a potent pro-inflammatory phenotype, the senescence-associated secretory phenotype (SASP). Recent studies have shown the importance of cytoplasmic DNA and chromatin, either reverse transcribed expressed retrotransposons or cytoplasmic chromatin fragments (CCF) expelled from the nucleus, in activation of nuclear SASP gene expression via the cGAS/STING cytoplasmic DNA-sensing pathway. As a source of chronic inflammation, over the long term SASP promotes tissue aging and disease. Thus, it is important to better define the mechanism of SASP activation in senescence. We show here that both the Promyelocytic Leukemia (PML) protein and HIRA histone chaperone are required for SASP expression in senescent cells. PML protein is the key organizer of PML nuclear bodies, nuclear features up to 1μM in diameter, containing many proteins and previously implicated in diverse cellular processes, including control of cell senescence and cellular intrinsic anti-viral immunity. HIRA is a histone chaperone best known for its ability to incorporate histone variant H3.3 into nuclear chromatin in a DNA replication-independent manner, including in non-proliferating senescent cells. HIRA localizes to PML nuclear bodies in senescent cells. We show that both HIRA and PML are required for activation of NF-kB and SASP. We found that HIRA regulates cytoplasmic NF-kB signaling in senescent cells through the CCF-cGAS-STING-TBK1 pathway. HIRA physically interacts with the autophagy cargo receptor p62 Sequestosome-1 (p62), and HIRA and p62 antagonistically regulate SASP. PML is required to maintain integrity of colocalized HIRA and p62 foci in the cell nucleus. Overall, our findings point to functions for HIRA and PML in coordination of cytoplasmic signalling and nuclear gene expression to regulate inflammation during cell senescence and aging.

Introduction

Senescence is a phenomenon characterized by irreversible growth arrest of a cell. Senescence not only causes proliferation arrest but also involves epigenetic and metabolic reprogramming, as well as a pro-inflammatory secretome called the senescence-associated secretory phenotype (SASP)(*1*). Senescence is considered a biomarker of aging and a key contributor to cell and tissue aging, leading to age-related diseases such as renal dysfunction, type-2 diabetes, Idiopathic pulmonary fibrosis (IPF), nonalcoholic fatty liver disease, osteoarthritis, and declining immune function (*2, 3*). SASP is recognized as a contributing factor to the development of senescence-related and age-related diseases, tissue damage, and degeneration. This is due to its ability to act as a source of chronic inflammation or "inflammaging" in aged tissue (*4*). The contribution of factors to the senescence-associated secretory phenotype (SASP) is dependent on the cellular context, although some key effectors and regulatory mechanisms are commonly shared. The transcription factor Nuclear Factor κB (NF-κB) functions as a "master regulator" of the SASP (*5*). Additionally, CCAAT/enhancer–binding protein beta (C/EBPß) and GATA4 have also been identified as important transcriptional regulators of the SASP (*2, 6, 7*). The SASP is regulated by various signaling molecules, including pathways such as p38 MAP-kinase, mTOR, JAK-STAT, and Notch, along with epigenetic regulators like G9a, GLP, MacroH2A, HMGB2, MLL1, BRD4, and H2A.J (*2, 6, 7*). SASP can also be regulated by DNA damage (*8*). We have observed a phenomenon in senescent cells whereby damaged DNA is expelled from the nucleus as cytoplasmic chromatin fragments (CCF) (*9*). This expulsion triggers the activation of SASP through the cytosolic DNA-sensing cGAS-STING-NF-κB pathway (*10-12*). Given that SASP is regulated at various levels, gaining a comprehensive understanding of its regulation is crucial. This understanding can pave the way for potential therapeutic approaches aimed at modulating SASP, which could promote healthy aging and alleviate the burden of senescence-associated diseases and degeneration.

Emerging evidence highlights the critical role of chromatin in integrating the SASP (*6*). Previously we found that the chromatin in senescent cells is maintained in a state of dynamic equilibrium, and the HIRA chaperone complex plays a critical role in regulating the chromatin landscape of these cells (*13*). The HIRA chaperone complex consists of HIRA, UBN1, and CABIN1, which work together with the histone-binding protein ASF1a to incorporate non-canonical H3.3 into chromatin in a manner that is independent of DNA replication (*13*). The deposition of H3.3 through the HIRA pathway has been firmly linked to genes that are actively being transcribed (*14*). Furthermore, it plays a crucial role in either activating or maintaining gene expression patterns in the long term (*15*). When cells undergo senescence, their chromatin can become condensed, resulting in the formation of senescence-associated heterochromatin foci (SAHF) (*16*). SAHF exhibit a distinct architecture comprising a core of constitutive heterochromatin encircled by a ring of facultative heterochromatin, with active chromatin located outside, and pericentromeric/telomeric regions positioned at the periphery (*17*). This suggests a process of spatial chromatin refolding within SAHF (*17*). Our observations have shown that HIRA plays a crucial role in the formation of SAHF (*18, 19*) and that the overexpression of HIRA is sufficient to induce SAHF formation (*18*). It was proposed that PML bodies serve as a molecular "staging ground" where HIRA complexes are assembled or modified before being translocated to chromatin and contributing to the formation of SAHF (*18, 19*). While we know that HIRA is linked to cellular senescence, the exact function of HIRA in senescence is still not fully understood.

Prior to the emergence of other senescence markers, such as cell cycle exit, SAHF, a large flat morphology, and SA β-Gal activity, HIRA enters within the subnuclear organelle promyelocytic leukemia nuclear bodies (PML NBs) during senescence induction, and this relocation is essential for SAHF formation (*18, 19*). A typical senescent nucleus contains 10-30 PML NBs, which are spherical structures of 0.2-1 μm in diameter (*18*). PML NBs play a versatile role in regulating a wide range of cellular activities, such as stress response, senescence, apoptosis, DNA repair, anti-viral immunity, and stem cell renewal (*20*). The PML tumor-suppressor protein acts as the primary scaffold of PML Nuclear Bodies (NBs), crucial for maintaining the structural integrity of these bodies (*21, 22*). PML interacts with numerous other partner proteins, referred to as 'client' proteins, to form the NBs (*22*). However, the clients are dispensable for PML NBs and diffuse more rapidly than the 'scaffold' PML protein (*22*).

PML can self-assemble through the binding of its conserved SUMO Interaction Motif (SIM) element to SUMOs (small ubiquitin-like modifiers) conjugated at multiple sites within the protein (*22*). The SUMO-SIM interactions are crucial for recruiting numerous client proteins to PML NBs, including transcription factors, DNA repair proteins, enzymes involved in post-translational protein modifications (*20, 22*). An intriguing characteristic among these partner client proteins is their ability to undergo SUMOylation in PML bodies (*20*). The level of PML protein increases in senescent cells (*23*), and has been reported to play a key role in senescence induction by repressing the expression of E2F target genes (*24*). In senescent cells, PML NBs are frequently found at the periphery of persistent DNA damage foci known as "DNA segments with chromatin alterations reinforcing senescence" (DNA-SCARS) (*8*). The integrity of these DNA-SCARS contributes to the regulation of SASP (*8*). Despite the presence of substantial evidence supporting the a role of PML in senescence phenotypes, its precise function remains unclear and elusive.

Given the co-localization of HIRA and PML in senescent cells, in this study we investigated their concerted involvement in senescence and made several noteworthy findings. Firstly, we found that HIRA and PML are essential for the expression of senescence-associated secretory phenotype (SASP) in senescent cells, but their role is not linked to growth arrest. Our experiments revealed that the localization of HIRA to PML bodies is critical for the expression of SASP. Additionally, we made an intriguing discovery of a novel non-canonical function of HIRA, independent of its histone deposition activity, in regulating SASP expression.

Results

HIRA and PML are required for SASP expression but not for proliferation arrest.

To begin to investigate the functions of HIRA and PML in senescence, we induced senescence in IMR-90 cells using etoposide and carefully monitored the accumulation of HIRA within PML bodies. During senescence, as previously shown by us and others (*18, 19, 23*), PML bodies were observed to become larger and more numerous, followed by the later accumulation of HIRA in PML bodies (Fig.S1a-d). This suggests that HIRA migrates towards PML bodies as senescence progresses. Next, we investigated whether HIRA functions as a client or scaffold protein in PML bodies. To test this, we disrupted the weak hydrophobic interactions in PML bodies of senescent cells using 1,6-hexanediol. This revealed that PML exhibited high resistance to dissolution in senescence, consistent with previous observations during viral infection (*25*). Therefore, PML acts as a scaffold protein in PML bodies in senescent cells (*22*). In contrast, HIRA was found to be a client protein, as evidenced by the immediate dissolution of HIRA foci within one minute (Fig.S1e). Investigating the association of PML bodies with DNA-SCARS by Super-Resolution confocal microscopy, we observed PML is not only at the periphery of the DNA-SCARS, rather it is frequently wrapped by DNA-SCARS (Fig.S1f-h). A peak in PML staining intensity corresponds to a trough in γH2AX. HIRA was found to be much more closely colocalized with PML than γH2AX (as shown in Fig.S1a-d) and was also wrapped by DNA-SCARS (Fig.S1i-k).

To investigate the role of HIRA and PML in senescence, we induced senescence after knocking down HIRA and PML using shRNA and performed RNA-seq analysis. The RNA-seq results revealed at least two notable gene clusters (Cluster 3 and 7; Fig.S2a, b) in terms of their dependence on HIRA and PML. Based on gene ontology analysis, the top predicted upstream regulators of cluster 3, including E2F4, MYC, E2F1, RB1, CCND1, and CDKN2A, were found to be associated with cell cycle pathways (Fig.S2c). Cluster 3 primarily consisted of genes that were related to promoting proliferation (*26*), which were repressed in senescent cells and similarly repressed in senescent cells depleted of HIRA and PML (Fig.S2d). This suggests that HIRA and PML are not necessary for the proliferation arrest observed in senescent cells (Fig. 1a, S2c, d). These findings were further confirmed by SA-β-Gal and EdU assays (Fig.S2e, f). In contrast, cluster 7 consisted of genes that showed upregulation during senescence and downregulation in cells lacking HIRA and PML (Fig.S2b, Fig.1b). Gene ontology analysis revealed that the top predicted upstream regulators of cluster 7, including TNF, IL1B, LPS, NF-κB complex, and IFNγ, were indicative of inflammatory pathways (Fig.1c). These findings strongly suggest that HIRA and PML are necessary for the expression of the senescence-associated secretory phenotype (SASP), which we confirmed using NanoString

nCounter technology, real-time qPCR, and western blotting of IL8 (Fig.1d-g). Furthermore, we observed that HIRA is essential for maximal SASP expression in various models of senescence, such as IR-induced senescence and oncogene-induced senescence (Fig.S2g, h).

To investigate a role for HIRA/PML organization in PML nuclear bodies (PML NBs) for SASP expression, we conducted an experiment using a low dose of the SUMO Activating Enzyme (SAE) inhibitor ML-792 to disrupt the organization of PML bodies, as previously reported (*27*). ML-792 impaired PML focal organization (Fig.1h, i), and dispersed the localization of HIRA (Fig.1h, j). Additionally, we made an interesting observation in senescent cells, whereby a low abundance higher apparent molecular weight form of HIRA was present (Fig.S2i). Inhibition of SUMOlylation using ML-792 led to the disappearance of this isoform (Fig.S2i). Knocking down SUMO-conjugating enzyme UBC9 with UBE2I siRNA also resulted in the disappearance of this polypeptide (Fig.S2j). This isoform was also absent in senescent cells lacking PML (Fig.S2k). These findings suggest that HIRA undergoes SUMOlylation within PML bodies in senescent cells. Our results also demonstrated that ML-792 was capable of suppressing the SASP, supporting the notion that the organization of HIRA/PML is necessary for SASP expression (Fig.1k).

In summary, our results demonstrate that while HIRA and PML are not essential for the arrest of proliferation, they play a crucial role in SASP expression. Moreover, the use of a drug-like inhibitor that disrupts the functional integrity of PML bodies by blocking SUMOylation (*27*) also suppressed the SASP, suggesting that SASP may depend on the co-localization of HIRA and PML.

Localization of HIRA in PML bodies is tightly linked to SASP expression.

Based on these findings, we aimed to more directly investigate whether the co-localization of HIRA and PML is required for the expression of SASP. To address this, we utilized a mutant form of HIRA called ***Δ***HIRA(520-1017) (referred to as ***Δ***HIRA), which has previously been shown to localize to PML bodies, disrupt the localization of endogenous HIRA to PML bodies, and exhibit dominant-negative inhibitory activity over HIRA function (*19*). We successfully expressed ***Δ***HIRA and confirmed its localization to PML bodies (Fig.2a, b). Furthermore, using an antibody that detects endogenous full length HIRA but not truncated ***Δ***HIRA (*19*), we observed that ***Δ***HIRA suppressed the localization of endogenous HIRA to PML bodies (Fig. 2c-f), while the number of PML bodies remained unchanged (Fig.2e). Importantly, ***Δ***HIRA demonstrated a significant blockade of the expression of various inflammatory cytokines, including IL1A, IL1B, IL6, and IL8, as determined by quantitative PCR (qPCR) and western blot (WB) analysis (Fig.2g, h). To further validate these findings, we performed RNA-seq analysis on senescent cells expressing ***Δ***HIRA and control cells. The results revealed a comparable number of differentially expressed genes (DEGs) in senescent versus proliferating cells in both the ***Δ***HIRA and wild-type samples, with 3821 genes upregulated and 3340 genes downregulated in the ***Δ***HIRA cells, and 3549 genes upregulated, and 3180 genes downregulated in the wild-type cells (Fig.S3a, b).

Remarkably, 35.6% of the genes (947/ (947+1712) X100) affected by both HIRA shRNAs and PML shRNA were also altered by ***Δ***HIRA. Specifically, the fold enrichment over random overlap was calculated as 33.47, with a p-value of less than $2.2X10^{-308}$ (two-tailed Fisher exact test) (Fig.2i). Furthermore, ***Δ***HIRA showed no effect on proliferation-related genes (*26*) but exhibited inhibition of SASP(*1*) (Fig.2j, k). Taken together, these results obtained with ***Δ***HIRA, in conjunction with those from the SUMOlyation inhibitor, strongly suggest that the proper spatial configuration of HIRA and PML bodies in senescent cells is crucial for the expression of SASP.

HIRA regulates SASP through activation of NF-κB pathway independent of it's H3.3 deposition role.

We set out to define the role of HIRA and PML in expression of SASP. Since NF-kB serves as the master regulator of SASP expression, we initially examined whether HIRA is necessary for NF-kB activation. We observed a decrease in NF-κB luciferase reporter activity in senescent cells depleted of HIRA (Fig.3a). This led us to propose that HIRA/PML might be essential for NF-kB transcriptional activity due to the requirement for transcription-coupled deposition of histone H3.3 at SASP genes facilitated by HIRA. To test this hypothesis, we asked whether

knockdown of HIRA would also impede the expression of SASP genes induced by stimuli other than senescence. We treated proliferating and senescent cells, with or without HIRA depletion through shRNA knockdown, with recombinant IL1A (rIL1A). To our surprise, and contrary to our hypothesis, we found that rIL1A effectively induced IL8 expression in both proliferating and senescent cells, irrespective of HIRA knockdown. In other words, the addition of rIL1A restored SASP expression in senescent cells lacking HIRA (Fig.3b, c), suggesting that HIRA-dependent transcription-coupled deposition of histone H3.3 is not essential for expression of these genes. To further investigate the requirement for deposition of histone H3.3 at SASP genes, we used siRNA to deplete H3.3 and assessed the expression of SASP genes such as IL8, IL1A, IL1B, and IL6. Remarkably, knockdown of H3.3 resulted in increased expression of these SASP genes compared to control senescent cells (Fig.3d, e). Consequently, we concluded that the requirement for HIRA/PML in SASP expression does not involve HIRA's role in transcription-coupled deposition of histone H3.3. We reasoned that HIRA and PML must be necessary for SASP expression upstream of gene transcription. Therefore, we examined the impact of HIRA knockdown on p65(RelA) nuclear translocation, phosphorylation, and other markers of NF-kB activation. Our results revealed that HIRA depletion in senescent cells led to suppressed p65(RelA) nuclear translocation (Fig.3f). Additionally, HIRA was crucial for the activation of the entire canonical NF-κB pathway, as evidenced by p65(RelA) phosphorylation, IKBα phosphorylation and degradation, and IKK α/β phosphorylation (Fig.3g). Furthermore, PML was also essential for p65(RelA) activation (Fig.3h). In conclusion, we determined that HIRA/PML is not required for transcription of NFkB target genes but is indispensable for signaling in senescent cells to activate NF-kB and subsequently induce SASP expression.

HIRA and PML are required for cGAS-STING-TBK1 signalling.

Numerous upstream factors have been implicated in the activation of NF-kB and SASP in senescent cells, including mTOR, GATA4, CEBPB, DDR, and cGAS/STING. However, upon closer analysis, we failed to observe a consistent effect of HIRA/PML on regulation of certain effectors involved in SASP, such as mTOR (reflected in p70S6K phosphorylation), GATA4, p38MAPK, CEBPB, and γH2AX (*7*) (Fig.S4). We hypothesized that HIRA is essential for the activation of the cytoplasmic CCF-cGAS-STING pathway, which in turn promotes NF-kB activation and SASP expression. Our observations revealed that both HIRA and PML play essential roles in TBK1 activation (Fig.4a-b), STING dimerization (Fig.4c), and cGAMP production (Fig.4d). Consistent with a role upstream of cGAS/STING activation, HIRA, primarily known for its nuclear localization, exhibited colocalization with cGAS in the cytoplasmic foci (CCF) (Fig.4e, f). Although HIRA was not necessary for CCF formation (data not shown), the absence of HIRA resulted in compromised enrichment of cGAS at the CCF (Fig.4g). Notably, we did not observe any changes in the expression of cGAS in cells lacking HIRA (data not shown). These findings suggest that HIRA regulates the cGAS-STING-TBK1-NF-kB axis through an unknown mechanism linked to regulated enrichment of cGAS at CCF. This highlights a novel role for HIRA in the cytoplasmic regulation of this pathway.

HIRA physically interacts with autophagy regulator p62, a repressor of SASP.

To investigate the non-canonical cytoplasmic role of HIRA in the expression of SASP, we conducted a study to identify potential effectors responsible for this function. We employed immunoprecipitation followed by mass spectrometry (IP-MS) on both proliferating and senescent cells to discover novel candidate effectors associated with SASP (Supplementary Excel File 1). Subsequently, we validated several candidates through immunoprecipitation followed by Western blotting (IP-WB), namely FHL2, LUZP1, PML, NBR1, SQSTM1 (p62), SP100, and MAGED1 (Fig.5a-c). Previously, we demonstrated the striking partial localization of p62 in CCF (*9*) (Fig.S5a). In this study, we further confirmed the interaction between HIRA and p62 through p62 immunoprecipitation (Fig.5d). Moreover, we observed the co-localization of p62 with HIRA in PML bodies in senescent cells (Fig.5e). Through siRNA knockdown experiments, we discovered that p62 functions as a robust negative regulator of SASP expression (Fig.5f). To validate this finding, we ectopically expressed p62, resulting in the potent suppression of SASP expression (Fig.5g). Ectopic expression of p62 not only dampened TBK1 activation, IL8 expression (Fig.5h), but also decreased cGAS levels in senescent cells (Fig.5i) and suppressed STING dimerization (Fig.5j). These results provide additional support for the role of p62 as a negative regulator of SASP expression. Knocking down p62 rescued SASP expression in HIRA-deficient cells, and knockdown of HIRA

decreased SASP in p62-deficient cells (Fig.5k), confirming the antagonistic regulatory roles of p62 and HIRA in SASP. In the absence of PML, we observed that the physical interaction between HIRA and p62 remained unchanged, as demonstrated by immunoprecipitation followed by Western blotting in PML-depleted cells (Fig.S5b, c). However, the absence of PML mislocalized both HIRA and PML (Fig.5l, m, S5d-f) and reduced the number of p62 foci in the nucleus (Fig.5n). Consequently, the absence of PML altered the spatial relationship between p62 and HIRA (Fig.5o).

To summarize, HIRA and p62 physically interact and they antagonistically regulate SASP expression. Additionally, our findings suggest that p62 controls the abundance of cGAS and signaling downstream of cGAS. PML, as a scaffold protein in PML bodies, facilitates the spatial organization between HIRA and p62.

Discussion

Senescent cells and their secretory phenotype known as the SASP contribute to a range of age-related conditions and diseases, such as atherosclerosis, osteoarthritis, cancer metastasis, cardiac dysfunction, myeloid skewing, kidney dysfunction, and overall decline in health span (*28*).To address the detrimental effects of senescent cells, two classes of candidate senotherapeutics have emerged. Senolytics selectively eliminate senescent cells or induce their death through senolysis, while senomorphics attenuate the harmful SASPs to mitigate the impact of senescent cells (*29*). It is important to note that the SASP is a complex and dynamic phenomenon, not representing a single phenotype. Its characteristics depend on the specific senescence inducer and the cell type involved (*28*). Multiple factors regulate the SASP, necessitating a comprehensive understanding of its regulation for the development of senomorphic drugs and interventions against age-related diseases. Our research aims to shed light on the regulation of SASP to contribute to this understanding.

In this study, we have demonstrated that the histone chaperone HIRA serves as a client protein, physically interacts with the PML protein, and localizes to PML bodies in senescent cells. This localization allows HIRA to regulate SASP expression without affecting cell proliferation arrest. Furthermore, our investigation revealed that HIRA exerts a non-histone chaperone role in the regulation of SASP, independently of its role in H3.3 deposition. In this process, HIRA directly interacts with the autophagy cargo receptor p62, which functions as a negative regulator of SASP. The p62 protein is able to downregulate cGAS. Since both cGAS and p62 are enriched in CCFs, it is probable that p62 mediates the degradation of cGAS within the CCF (*30*), thereby reducing the interaction between CCF and cGAS. Additionally, it can be speculated that the physical interaction between HIRA and p62 somehow restores cGAS within the CCF. This subsequent activation of the cGAS-STING-TBK1-NF-kB signaling axis leads to the expression of SASP, which requires further investigation. In the absence of PML, HIRA and p62 foci become diffused within the nucleus, potentially disrupting the normal spatial and regulatory relationship between HIRA and p62.

Multiple reports describe the induction of PML during senescence, suggesting its correlation with the inhibition of E2F gene expression, which is proposed to induce senescence (*23, 24*). However, in our observations, although PML is induced at the protein level in senescent cells, the number and intensity of PML foci increase, but it is not essential for proliferation arrest. Moreover, in the absence of PML, E2F target gene expressions remain dampened (Fig S2c,d). This suggests that although PML induction and E2F target gene repression are correlated, PML is not essential in all contexts for repression of E2F target genes.

It is well established that PML bodies are associated with the interferon system and play a crucial role in anti-viral defense (*31*). The cGAS/STING pathway is also involved in anti-viral defense. Upon binding to viral double-stranded DNA, cGAS initiates a tightly regulated signaling cascade involving the adapter STING (*10, 32*). This cascade triggers various inflammatory effector responses by activating transcription factors including IRF3 and NF-kB (*10, 32*). Here, we have shown that PML is also involved in cGAS/STING signaling and expression of SASP in response to another type of cytoplasmic DNA, CCF. Previous research conducted by our laboratory has demonstrated that HIRA is also engaged in the detection of

foreign viral DNA (*33*). Moreover, HIRA actively participates in antiviral functions by promoting the expression of cellular genes associated with innate immunity and a diverse array of interferon-stimulated genes (ISGs)(*34*). Here we have also observed the presence of HIRA within CCFs. In the process of senescence, as well as during DNA virus infection, DNA transfection, and interferon treatment, HIRA accumulates in PML bodies (*18, 33*). Thus, HIRA responds to foreign and cytoplasmic DNAs in a way that links it to PML. PML and HIRA's localization to PML bodies are required for expression of SASP. Therefore, the shared involvement of HIRA, PML, cGAS, and STING in cellular senescence and intrinsic antiviral immunity suggests that "seno-viral" signaling acts as a nexus linking cellular innate immunity and cell senescence.

PML within nuclear bodies (NBs) has been suggested to finely regulate various processes by facilitating posttranslational modifications, particularly SUMOylation, of partner client proteins, including PML itself (*20, 35*). SUMOylation of PML is a prerequisite for NB formation (*36*) and SUMOylation of partners can lead to partner sequestration, activation, or degradation, thereby influencing a wide range of cellular functions including senescence (*20, 35, 37, 38*). The overexpression of SUMO has been found to induce senescence, as increased SUMOylation of specific target proteins can lead to premature cellular senescence (*37, 38*). Our preliminary data suggests that in addition to PML, HIRA is also likely to undergo SUMOylation. SUMOylation requires the presence of a consensus SUMOylation motif within the target protein. By performing bioinformatic analysis, we have identified several potential SUMOylation sites within the HIRA protein, such as K92, K617, K809, and K843. However, further investigation is needed to confirm the occurrence of HIRA SUMOylation and determine the sites and function of SUMOylation during senescence. Based on our findings, we propose that HIRA translocates to PML bodies in senescent cells for the purpose of SUMOylation, which significantly influences its functionality. It is noteworthy that the absence of HIRA does not alter the number of PML NBs, yet it leads to a decrease in SASP expression. Hence, in the HIRA/PML axis, HIRA plays a pivotal role in expressing SASP, while PML NBs appear to act as a molecular platform for spatial interaction of HIRA with other clients, such as p62, and post-translational modification, SUMOylation in particular. Considering the increasing recognition of the significance of senescence, SUMOs, and PML in cancer development and therapeutic response (*38*), this finding represent exciting development, warranting thorough exploration and study.

Recent research has emphasized the importance of p62 in senescence and SASP regulation. The p62 protein acts as a negative regulator of SASP in GATA4-mediated NF-κB activation (*39*), which aligns with the findings of our study. Furthermore, p62 functions as a cargo receptor for the degradation of proteins in the inflammation pathway. During viral infection or dsDNA stimulation, p62-mediated autophagy facilitates the degradation of cGAS, STING, and IRF3, which are key components of the cGAS-STING pathway (*30, 40-42*). Consequently, p62 exerts negative control over the cGAS-STING pathway, thereby regulating type I IFN signaling during virus infection (*30, 41, 42*). However, in the case of dsDNA stimulation, STING is specifically degraded through a p62-dependent mechanism (*41*). Although p62 does not directly bind to cGAS-associated dsDNA, it predominantly colocalizes with STING upon dsDNA transfection (*41*). In contrast, p62 is abundant in cGAS-bound CCFs, suggesting p62 may mediate the degradation of cGAS associated with CCF, as suggested by p62 overexpression in senescent cells. While the exact role of p62 and cGAS degradation in this study is not fully elucidated, it is speculated that the physical and spatial interaction between p62, HIRA, and PML regulates the CCF-cGAS-STING-NF-κB axis in senescence. Ongoing and future studies will address these questions. The inclusion of p62 in both the HIRA/PML axis and cGAS-STING pathway in senescence and antiviral signaling provides additional support for the concept of "seno-viral" signaling and suggests an evolutionary connection between viral infection and senescence.

In summary, this study points to a novel cytoplasmic role of HIRA in the cGAS-STING signaling pathway in senescent cells, and reveals a shared role for HIRA and PML in control of SASP, likely mediated by PML's role in organizing the spatial configuration of HIRA and p62,

antagonistic regulators of SASP. The findings strengthen the connection between cytoplasmic/foreign DNA sensing mechanisms in virus infection and senescence and highlight the potential therapeutic significance of targeting this pathway to suppress inflammatory responses.

Materials and Methods

Primers, Plasmids, and antibodies

A comprehensive list of the primers, plasmids and antibodies used in the study can be found in the supplementary files.

Cell culture and inducing senescence.

To culture the cells and induce senescence, primary human IMR-90 fibroblasts were grown in DMEM supplemented with 10% FBS, 100 U/mL penicillin, 100 µg/mL streptomycin, and 2 mM glutamine at 37°C in a humidified atmosphere with 5% CO2 and 3.5% oxygen. To induce senescence, cells were treated with etoposide, a DNA damaging agent, at a concentration of 25 or 50 µM for 24 hours. Following this treatment, the etoposide-containing media was replaced with complete media. After eight days, the cells were harvested for senescence assays.

Drug treatment in senescent cells

After treating with etoposide, the cells were exposed to SUMOlyation inhibitor drug by replacing the etoposide-containing media with media containing ML-792 (MedChemExpress). The old media were then substituted with new media that contained vehicle and drugs at intervals of 2-3 days. Following eight days of drug treatment, the cells were collected to perform various assays.

Retrovirus Production

Retroviral plasmids was used for the ectopic expression of HA-HIRA(*19*), HA-**Δ**HIRA(520-1017)(*19*), and pBABEpuro-HA-p62 (Addgene:71305). Retrovirus production was performed by the SBP Functional Genomics Core Facility using a three-plasmid system consisting of retroviral vector, retro-Gag-Pol, and VSVG, as described earlier (*43*). HEK293T cells were co-transfected with the plasmids, and transfected cells were refed with DMEM supplemented with 2.5% FBS. Virus supernatant was collected every 24 hours from the 2nd to 4th day post transfection, and the crude viral supernatant was pooled and filtrated through 0.22-µm membrane. The concentrated viral particles were then purified using 20% sucrose gradient ultracentrifugation at 21,000 rpm for 2 hours, and the resulting pellet was resuspended in 1XPBS, aliquoted, and stored at −80°C. IMR-90 cells were infected with a concentrated viral suspension in the presence of 8 µg/mL polybrene, undergoing two infection cycles for a total duration of 24 hours. The infected cells were then selected using 1 µg/mL puromycin.

Lentivirus Production

The pLKO.1 lentiviral transduction system was used for knocking down HIRA, PML, and SQSTM1/p62. To expresses NF-**κ**B luciferase reporter cells, pHAGE NFkB-TA-LUC-UBC-GFP-W lentiviral plasmid (Addgene plasmid # 49343**)** was used. To produce lentiviral particles, HEK293T cells were transfected with the pLKO.1 constructs and packaging plasmids using Lipofectamine 2000 (Thermo Fisher Scientific). After six hours, the transfection medium was replaced with fresh culture medium. At 24 and 48 hours post-transfection, the viral supernatants were collected, filtered through a 0.45-µm-pore-size PVDF filter (Millipore), and concentrated by centrifugation at 45,000X g for two hours at 4°C. For infection, IMR-90 cells were incubated with the concentrated viral suspension containing 8 µg/mL polybrene for a duration of 20 hours. The infected cells were subsequently selected using 1 µg/mL puromycin. The shRNA sequences are provided in the supplementary files.

si-RNA Transfection

To suppress gene expression in senescent cells, a method involving the transfection of 20 nM Dicer-Substrate Short Interfering RNAs (DsiRNAs) from IDT was employed. This transfection

was carried out using Lipofectamine™ RNAiMAX (Invitrogen) following the manufacturer's protocol, 24 hours after the administration of Etoposide treatment. The following day, the transfection media was replaced with complete DMEM media, and the cells were collected for analysis after 7-8 days of Etoposide treatment. The following DsiRNAs were used for knocking-down: HIRA (hs.Ri.HIRA.13.1, 13.3); PML (hs.Ri.PML.13.1, 13.2); SQSTM1/p62 (hs.Ri.SQSTM1.13.4,13.5, 13.6); UBC9 (hs.Ri.UBE2I.13.1, 13.3); H3.3 (pool of H3F3A, H3F3B siRNAs, hs.Ri. H3F3A.13.1,13.13; hs.Ri. H3F3B.13.1,13.2). The ON-TARGETplus Human PML siRNA SMARTPool from Dharmacon was also used for PML knockdown.

SA- β-Gal assay

The Senescence-associated β-Gal Staining method was adapted from Debacq-Chainiaux et.al (*44*). In brief, the cells were fixed at room temperature for 5 minutes in a solution containing 2% formaldehyde and 0.2% glutaraldehyde in PBS. The cells were washed twice with PBS. Subsequently, they were overlaid with a freshly made staining solution and incubated at 37°C for 5-7 hours in a non-CO2 incubator. The staining solution consisted of the following components: 40 mM Na2HPO4 at pH 6, 150 mM NaCl, 2 mM MgCl2, 5 mM K3Fe(CN)6, 5 mM K4Fe(CN)6, and 1 mg/mL X-gal in DMSO. After staining, the cells were rinsed with PBS and then with water to remove salt. The number of β-Gal positive cells was counted under a phase contrast microscope.

Edu Assay

The Edu assay was performed based on the method described by Salic and Mitchison (*45*). EdU was introduced into the cell media to achieve a final concentration of 10 μM in 24-well plates. Following a 4-hour incubation period, the cells underwent cross-linking with a 10% formalin solution at room temperature for 15 minutes. After aspirating the formalin solution, the cells were subjected to three washes with TBS/0.5% Triton X-100 to permeabilize the cells and quench the formaldehyde. A mixture was prepared, consisting of 2 mL of TBS/0.5% Triton X-100, 2 μL of 50 mM FAM-N3 (6-Carboxyfluorescein Azide) in DMSO, 20 μL of 100 mM CuSO4, and 200 μL of 1.0 M sodium ascorbate. The labeling solution was added to cover the cells adequately, and the mixture was incubated in the dark at room temperature for 30 minutes. Subsequently, the cells were washed three times with TBS/0.5% Triton X-100 and once with PBS. Finally, the cells were stained with DAPI and mounted on slides.

Quantitative real-time PCR

The TRIzol method was used to extract total RNA according to the manufacturer's instructions (Invitrogen). cDNA was prepared from 1 μg of extracted RNA using RevertAidTM reverse transcriptase (Thermo Scientific) according to the manufacturer′s protocol. Quantitative real-time PCR was performed using the PowerTrack™ SYBR Green Master Mix (Applied Biosystems) on the QuantStudio 6 Flex Real-Time PCR Systems (Applied Biosystems). The fold change was calculated using the 2^(-ΔΔCt) method on triplicate samples, with GAPDH serving as the housekeeping gene. The primer sequences are provided in the supplementary files.

NanoString analysis

Nanostring nCounter analysis was employed to assess SASP gene expression, as previously mentioned (*46*). The purified RNA was analyzed on an Agilent 2200 TapeStation using RNA screentape. Subsequently, the samples were run on an nCounter platform using either the nCounter custom human SASP panel, which consisted of 31 canonical SASP genes (*1*) and three internal reference genes. The hybridization reactions were carried out following the manufacturer's instructions from NanoString Technologies. To ensure data quality, field of view counts and binding density measurements were manually extracted from the data and checked against the manufacturer's protocol to ensure acceptability. Differential expression analysis was conducted using either nSolver to determine log2 fold changes and p-values, which were obtained using Student's t-test. p-values below 0.05 were considered statistically significant. Heat maps illustrating the normalized counts of specific gene subsets were generated using GraphPad Prism v9.

RNA sequencing and analysis

For RNAseq experiments, the RNA extracted using the TRIzol method was further purified using the ammonium acetate precipitation method (Ambion, Catalog: AM9070G). The quality of RNA was assessed using Tapestation from Agilent Technologies. RNA-seq libraries were prepared either by the Genomics Core at SBP Medical Discovery Institute, San Diego or by Novogene, Sacramento, following standard Illumina protocols. RNA-sequencing was conducted as single-read 75 nucleotides in length on the Illumina NextSeq500 platform by the Genomics Core at SBP Medical Discovery Institute (Fig.1), or on the Illumina NovaSeq PE150 platform (6 G raw data per sample) by Novogene (Fig.2).

Raw fastq files were aligned to hg19 (shHIRA/PML RNAseq) or hg38 (DHIRA RNAseq) (DHIRA represents *Δ*HIRA) using STAR 2-pass pipeline (*47*). Reads were filtered, sorted and indexed by SAMtools (*48*). FPKM were generated using CuffLinks for downstream visualization(*49*). Genome tracks (bigWig files) were obtained by Deeptools (*50*). Raw read counts were obtained by HTSeq for differential analysis (*51*). Differentially expressed genes were obtained by DESeq2 (*52*).

RNA sequencing data were uploaded to GEO under accession numbers GSE233327 and GSE233847.

Immunoblotting

The Western blotting technique was previously described (*46*). For cell lysis, cells were treated with either SDS sample buffer (composed of 62.5 mM Tris at pH 6.8, 0.01% bromophenol blue, 10% glycerol, and 2% SDS) or EBC500 buffer (containing 50 mM Tris-HCl at pH 8.0, 500 mM NaCl, and 0.5% NP40). For immunoblotting of STING dimer, cells were lysed in buffer containing 50 mM Tris pH 7.5, 0.5 mM EDTA, 150 mM NaCl, 1% NP40, 1% SDS without any reducing reagent (*10*). The proteins were then separated on a 4%-12% Bis-Tris gel (NuPAGE, Thermo Fisher Scientific) through electrophoresis and subsequently transferred to a PVDF membrane. Next, the membranes were blocked in a solution consisting of 5% milk supplemented with 0.1% Tween 20 (TBST) for 1 hour at room temperature. Following the blocking step, the membranes were incubated with primary antibodies overnight at 4°C. The primary antibodies were diluted in 4% BSA in TBST. Afterward, the membranes were washed three times with TBST and incubated with horseradish-peroxidase-conjugated secondary antibodies at room temperature for 1 hour in a solution of 5% milk/TBST. Following another round of washing three times with TBST, the antibody binding was visualized using either SuperSignal™ West Pico or Femto Substrate (Thermo Scientific). All information regarding the antibodies used is provided in the supplementary files.

NF-*κ*B Luciferase reporter assay

After lentiviral transduction of the lenti-NF-κB-luc-GFP system, IMR-90 cells were further infected with TRC control and two HIRA shRNA-producing pLKO.1 lentivirus particles. Following puromycin selection, the cells were seeded in 24-well plates, and senescence was induced with Etoposide. After seven days, the cells were washed twice with 1X phosphate-buffered saline (PBS) and lysed using 1X passive lysis buffer (Promega). The luciferase activity was measured using the dual luciferase assay kit (Promega) according to the manufacturer's protocol. Briefly, the lysate was clarified by brief centrifugation, and the firefly luciferase reporter activity in the clear supernatant was measured using a Clariostar Multi-Mode Microplate Reader. GFP fluorescence in the same lysate was measured using the same reader as a normalization control.

cGAMP Assay

The 2’3’-cGAMP ELISA Kit (Catalogue no. 501700) from Cayman Chemical was used to quantify 2’3’-cGAMP in the cell lysate following the manufacturer’s protocol. To prepare the cell lysates, Mammalian Protein Extraction Reagent (M-PER™, ThermoFisher Scientific, Catalogue no. 78501) was used. Each sample or standard (50 µL) was added to the appropriate wells of the 2’3’-cGAMP ELISA plate, which was then incubated overnight at 4 ºC with 2’3’-cGAMP-HRP tracer and 2’3’-cGAMP ELISA Polyclonal Antiserum. The plate was

washed, and TMB Substrate was added, followed by incubation for 30 minutes at room temperature in the dark. Finally, Stop Solution was added to each well, and the absorbance was measured at 450 nm using a microplate reader.

Immunofluorescence Microscopy

Cells were cultured either on cover slips in 24-well plates or in a 96-well plate (PhenoPlate, PerkinElmer) and fixed with 4% paraformaldehyde in PBS for 10 minutes at room temperature. Following fixation, the cells were washed three times with PBS, and the cells were permeabilized with PBS + 0.2% Triton X-100 for 4 minutes at room temperature. Next, the cells underwent blocking with the blocking buffer (PBS + 4% BSA + 1% goat serum) for 1 hour at room temperature, followed by incubation with primary antibodies in blocking buffer for 90 minutes at room temperature. After the incubation, the cells were washed three times with PBS + 1% Triton X-100 and then incubated with secondary antibodies, which were prepared in blocking buffer, for two hours at room temperature. After washing three times with PBS, DAPI (200 ng/mL) in PBS was added for nucleus staining. The cells were incubated for 5 minutes at room temperature in the dark for staining and were subsequently washed three times with PBS. Finally, for coverslips, pre-warmed mounting medium was added to a clean glass slide, and the coverslip with the cells facing down was inverted onto the medium. The edges were sealed with fingernail polish and allowed to dry. The plates or slides were stored at 4°C in a dark environment. In certain nuclear staining experiments, cells were prewashed with EBC lysis buffer (50 mM Tris HCl pH 8.0 + 120mM NaCl + 0.5% NP40 + 5 mM MgCl2 + Protease Inhibitors cocktail) for 30 seconds to reduce the cytoplasmic background before fixation. All information regarding the antibodies used is provided in the supplementary files.
Most of the images were taken automatically in an unbiased manner using a motorized platform by the Nikon Eclipse Ti2 epifluorescence microscope. The image data were processed with Nikon NIS-Elements.

Airyscan Super-Res microscopy

High-resolution z-stack images of cells were captured using a ZEISS 880 LSM Airyscan confocal system with an upright stage and a 63x 1.4 NA oil objective. The imaging parameters included a pixel dwell time of 2.05 µs, a pixel size of 20 nm/pixel in SR mode (with a virtual pinhole size of 0.2 AU), and a z-spacing of 0.159 µm. The zoom factor ranged from 2.6 to 3.4. ZEISS Zen software was used to process the images with the Airyscan parameter determined by auto-filter settings. For senescent cells, the Airyscan parameter was increased by 15% compared to the auto-filter settings. DAPI, Alexa Fluor 488, and Alexa Fluor 594 were imaged using the 405 nm, 488 nm, and 561 nm lasers, respectively. Laser power and detector gain were optimized for each staining condition.

Cellular fractionation

For cellular fractionation, NE-PER™ Nuclear and Cytoplasmic Extraction Reagents (Catalog: 78835) were used according to manufacturer's protocol. Briefly, cells pellets were collected as dry as possible by trypsin-EDTA method. To proceed with cytoplasmic and nuclear protein extraction, ice-cold CER I was added to the cell pellet, maintaining the specified reagent volumes. The tube was vortexed vigorously for 15 seconds and then incubated on ice for 10 minutes. Afterward, ice-cold CER II was added to the tube, followed by vortexing for 5 seconds and incubation on ice for 1 minute. The tube was vortexed again for 5 seconds and centrifuged at 16,000 × g in a microcentrifuge for 5 minutes. The supernatant, which contained the cytoplasmic extract. The insoluble fraction containing nuclei was suspended in ice-cold NER and vortexed for 15 seconds. The sample was placed on ice and vortexed every 10 minutes for a total of 40 minutes. Afterward, the tube was centrifuged at 16,000x g in a microcentrifuge for 10 minutes. The resulting supernatant, representing the nuclear extract.

Immuno-precipitation

To pull down HIRA-interacting proteins, a cocktail of mouse monoclonal antibodies (WC15, WC19, WC117, WC119) in approximately equimolar proportions was utilized (*13*). For SQSTM1/p62-interacting proteins, an Anti-p62 (SQSTM1) Rabbit polyclonal antibody (MBL, PM045) was used.

First, the cells were scraped from 150-cm2 plates and suspended in 1 mL of EBC500 buffer (50 mM Tris-HCl, pH 8.0; 500 mM NaCl; 0.5% NP40) containing Protease and Phosphatase Inhibitor Cocktail. The resulting lysate was rotated for 30 minutes at 4°C on a rotator and then centrifuged at 12,000x g for 10 minutes at 4°C to eliminate cellular debris. The protein concentration of the lysate was determined using the BCA method. For the immunoprecipitation step, Dynabeads™ Protein G (Thermo Fisher Scientific, Catalogue No. 10004D) were utilized. A volume of 25 µL of Dynabeads per mg of protein was employed, and 2 mL Eppendorf Protein LoBind Tubes were used throughout the procedure. The pooled beads were initially washed twice with 0.5% NP-40 in TBS. Subsequently, the beads were exposed to the antibody for the target protein and isotype control, with a total volume adjusted to 500 µL. The antibody and beads were incubated for 45 minutes at room temperature on a rotator. Following the incubation, the beads were washed three times with 0.5 mL of 0.5% NP-40 in TBS to remove any unbound antibody. The antibody-bound beads were then added to the lysate and incubated overnight at 4°C on a rotator. Prior to adding the beads, a portion of the lysate was removed to prepare input samples. On the subsequent day, the beads underwent washing either five times with cold NETN buffer (20 mM Tris, pH 8; 1 mM EDTA; 0.5% NP40; 100 mM NaCl) for immunoprecipitation followed by western blot (IP-Western blot), or three times with cold NETN buffer, followed by two times with TBS buffer for immunoprecipitation-mass spectrometry (IP-MS). The DynaMag™-2 Magnet (Thermo Fisher Scientific, Catalog number: 12321D) was used for all the washes.

For IP-MS, 10% of the immunoprecipitation solution was collected during the last wash intended for IP-Western blot. The remaining 90% of the beads were collected and subjected to snap-freezing after removing all liquid. Additionally, a western blot was conducted using the 10% aliquot to ensure the quality of the immunoprecipitation prior to mass spectrometry analysis.

Immunoprecipitation-mass spectrometry (IP-MS)

Mass spectrometry analysis of immunoprecipitated proteins was performed by the Proteomics Core at SBP Medical Discovery Institute, San Diego. Immunoprecipitated proteins on beads were treated with urea and ammonium bicarbonate, followed by reduction and alkylation of disulfide bonds and cysteines. After overnight digestion with Trypsin/Lys-C mix (Promega), peptides were transferred, acidified, desalted, and quantified using NanoDrop. The remaining sample was dried using SpeedVac concentrator.

Dried peptides were resuspended in 2% acetonitrile, 0.1% formic acid and analyzed using a NanoDropTM spectrophotometer. LC-MS/MS analysis was performed using a Proxeon EASY-nanoLC system coupled to a Q-Exactive Plus mass spectrometer. Peptides were separated on an analytical C18 Aurora column with a 120-min gradient. MS1 spectra were measured in the Orbitrap with a resolution of 70,000, and MS2 spectra were acquired using HCD fragmentation with a resolution of 17,500. Dynamic exclusion and other parameters were set accordingly. Data analysis utilized MaxQuant software version 1.6.11.0, searching mass spectra against the Homo sapiens Uniprot protein sequence database and GPM cRAP sequences. A 1% false discovery rate (FDR) filter was applied for spectrum and protein identification.

Statistics

The statistical significance was analyzed utilizing GraphPad Prism 9 Software. In most cases, the value for the proliferation control was considered as 1, following convention, and the fold change of senescent cells was calculated. To determine whether the fold change significantly differed from 1, the one-sample t-test was employed. When comparing two datasets, unpaired two-tailed Student's t-test was performed. For the comparison of more than two datasets, the one-way ANOVA test was used. A significance level of $p<0.05$ was considered to determine statistical significance. The data are expressed as Mean±SD from three biological replicates and are representative of at least two independent experiments. The symbols #,*, **, ***, **** indicate significance levels of $p<0.01$, $p<0.05$, $p<0.01$, $p<0.001$,and $p<0.0001$, respectively.

Figure legends

Figure 1: HIRA and PML are required for SASP expression but not for proliferation arrest. (a) Heatmap of RNA-seq analysis showing the expression of proliferation-associated genes (Cluster 3) and (b) inflammatory pathway genes (Cluster 7) in proliferating (Pro) TRC control and senescent IMR90 cells (control and HIRA, PML-deficient cells) 8 days after Etoposide treatment. Color intensity represents the log2 fold change, with red indicating high expression and blue indicating low expression. (c) Top upstream regulators of Cluster 7 identified by IPA analysis. (d) Heatmap of NanoString analysis and (e) Real-time qPCR analysis showing the expression of SASP genes in control (TRC) and HIRA (sh1,sh2), and PML (sh-PML) deficient cells. (f) Western blot analysis of IL-8 as a SASP marker, and p21 and p16 as senescence markers in HIRA-deficient senescent cells and (g) in PML-deficient senescent cells using si-RNA. NC denotes negative control si-RNA (h) Representative immunofluorescence image showing the localization of HIRA and PML in senescent cells in the presence of drug ML-792. (i,j) Quantification of the number of PML and HIRA foci in senescent cells in the presence of drug ML-792, respectively. (k) Real-time qPCR analysis of SASP genes in the presence of ML-792. Data shown in (a), (b), (d), (e), and (k) represents three biological replicates. Figures (e,i,j,k) represent the mean ± SD. The p-values were calculated using an unpaired two-tailed Student's t-test (e,k), and using one-way ANOVA with Dunnett's multiple comparisons test (i,j). The random images were captured automatically using Nikon motorized platform. The values were calculated using Nikon NIS-Element software from 3 different wells with multiple fields. (∗∗∗) $p < 0.001$; (∗∗) $p < 0.01$; (∗)$p < 0.05$.

Figure 2: Localization of HIRA in PML bodies is tightly linked to SASP expression.
(a) Expression of empty vector (EV), wild-type HIRA (FL), and ΔHIRA(520-1017) in senescent IMR-90 cells by western blot. The predicted molecular weight of HIRA (FL) is 112 kDa, while ΔHIRA is expected to be 55 kDa. (b) Representative immuno-fluorescence images showing ΔHIRA expression in senescent cell nuclei, stained with HA antibody. (c) Representative immuno-fluorescence images illustrating the localization of endogenous HIRA in control (EV) and ΔHIRA cell lines. The WC119 antibody used to detect endogenous HIRA does not recognize ΔHIRA (520-1017)(*19*). Figures (d-f) represent the number of HIRA foci, PML foci, and their ratio, respectively. Data represents the mean ± SD. The values were automatically calculated using Nikon-NIS software from three different wells with multiple fields in an unbiased manner. (g) Real-time qPCR analysis showing the expression of SASP genes in control (EV) and ΔHIRA senescent cells. Data shown represents the mean ± SD of n = 3 biological replicates. (h) Immunoblot analysis of IL8 as a SASP gene, Cyclin A as a proliferation marker, and p21, p16 as senescent markers in control (EV) and ΔHIRA senescent cells. (i) Venn diagram depicting differentially expressed genes (DEGs) in ΔHIRA, two HIRA-knocked-down, and one PML-knocked-down senescent cells, generated using VENNY2.1.
Heatmap of RNA-seq analysis displaying the expression of (j) proliferation genes (*26*) ; and (k) SASP genes (*1*) in proliferating control (EV (Pro)), senescent control (EV), and senescent ΔHIRA cells, 8 days after Etoposide treatment. Color intensity represents the log2 fold change, with red indicating high expression and blue indicating low expression. Data shown represents n = 3 biological replicates. For data (d-g), the p-values were calculated using an unpaired two-tailed Student's t-test. (∗∗∗) $p < 0.001$; (∗∗) $p < 0.01$; (∗) $p < 0.05$, (#) $p<0.1$.

Figure 3: HIRA regulates SASP through activation of NF-κB pathway independent of it's H3.3 deposition role. (a) The relative luminescence was measured from the lysate obtained from lenti-NF-κB-luc-GFP reporter IMR-90 cells. The luciferase activity was normalized by calculating the mean fluorescence of GFP. (b,c) Real-time qPCR analysis was conducted to measure the expression of HIRA as an indicator of knock-down efficiency and IL-8 as SASP genes in proliferating and senescent control cells (sh-Luc control) and HIRA-deficient cells (sh1, sh2-HIRA) after treatment with recombinant IL-1α (20 ng) for 24 hours. (d) Immunoblot analysis was performed on proliferating control cells (NC), senescent control cells (NC), and H3.3 knock-down cells. (e) Real-time qPCR analysis was conducted to assess the expression of SASP genes in control (NC) and H3.3-deficient senescent cells (si-H3.3). (f) The nuclear

translocation of p65 was analyzed by cellular fractionation followed by western blotting. α-Tubulin was used as a cytoplasmic marker, and Lamin A/C was used as a nuclear marker. (g) The canonical NF-κB pathway was analyzed by immunoblotting in HIRA-depleted cells (h) Immunoblot analysis was performed to examine p65 phosphorylation in PML-depleted cells. Both TRC and sh-Luc were used as control samples. Data shown in (a-c), and (e) represents the mean ± SD of n = 3 biological replicates. The p-values were calculated using an unpaired two-tailed Student's t-test. (***) $p < 0.001$; (**) $p < 0.01$; (*) $p < 0.05$.

Figure 4: HIRA and PML are required for cGAS-STING-TBK1 signalling.
(a,b,c) Cell lysates were subjected to immunoblotting. STING blot was performed under non-reducing condition. * indicates STING dimer. (d) cGAMP synthesis was assessed using the ELISA method after 8 days of Etoposide treatment. Data represent the mean ± SD of n = 6 (3 biological replicates from two independent experiments). The p-values were calculated using one-way ANOVA with Dunnett's multiple comparisons test. (e,f) Representative images of Airyscan Super-Resolution microscopy of HIRA in CCF. (g) Cells were stained for DAPI, γH2AX, and cGAS in control (NC) and HIRA-deficient cells (si1,2-HIRA). The cGAS intensity in individual CCF (DAPI and γH2AX positive foci in cytoplasm) was calculated. Each data point represents an individual CCF. The values were calculated using Nikon NIS-Elements software from 3 different wells with multiple fields. The p-values were calculated using an unpaired two-tailed Student's t-test. (****) $p < 0.001$;(***) $p < 0.001$; (**) $p < 0.01$; (*)$p < 0.05$.

Figure 5: HIRA physically interacts with autophagy regulator p62 to regulate SASP expression. (a-c) Validation of HIRA interactor proteins by western blotting, obtained from IP-MS. (d) Immunoprecipitation of p62 interactor proteins followed by immunoblotting for HIRA. Short exposure (SE) and long exposure (LE) were performed. (e) Representative image showing the localization of p62 with HIRA in PML bodies of senescent cells. (f) Real-time qPCR analysis showing the expression of SASP genes in control (NC) and p62-deficient cells (si1, si2, and si3). (g) Real-time qPCR analysis showing the expression of SASP genes and (h,i) Immunoblot analysis of cytoplasmic fraction of senescent empty vector (EV) and HA-p62 expressing cells. (j) STING immunoblot was performed under non-reducing conditions. * indicates STING dimer. (k) Real-time qPCR analysis showing the expression of SASP genes after 7 days of 25 μM etoposide treatment. IMR-90 cells were first infected with lentivirus expressing shRNA against p62 (sh1 and sh2) and control (sh-Luc). The following day of Etoposide treatment, the cells were transfected with negative control siRNA (NC) and si-HIRA. (l) Representative image showing the localization of p62 with HIRA in the absence of PML bodies in senescent cells. (m-o) The random images were captured automatically using Nikon motorized platform. The values were calculated using Nikon NIS-Element software from 3 different wells with multiple fields. Data in (f) and (k) represent the mean ± SD of n = 3 biological replicates, (g) represents three biological replicates from two independent experiments (n=3X2). For data in (f), (g), and (k), the p-values were calculated using an unpaired two-tailed Student's t-test. (****) $p < 0.0001$; (***) $p < 0.001$; (**) $p < 0.01$; (*) $p < 0.05$.

Figure S1: HIRA acts as a client protein in PML bodies in senescent cells.
(a-d) Super-resolution images of HIRA-PML kinetics were captured after 0, 1, 3, 5, and 7 days of treatment with 50 μM Etoposide. (e) Representative images of senescent cells were treated with 1% 1,6-hexanediol for the indicated time periods (f) Super-resolution images of DNA-SCARS around PML bodies in senescent cells. (g,h) Line scan analysis was performed using ImageJ software. (f) Super-resolution images of DNA-SCARS around HIRA in senescent cells. (j,k) Line scan analysis was performed using ImageJ software. All super-resolution images were acquired using a ZEISS 880 LSM Airyscan confocal system (63x 1.4 NA oil objective).

Figure S2: HIRA and PML are necessary for SASP expression but not for proliferation arrest in different senescence models.
(a-b) Clustering analysis of RNA-seq data reveals distinct gene expression patterns in different clusters. (c) Gene ontology analysis identifies top upstream regulators in Cluster 3. (d) Heatmap representation of proliferation genes expression (*26*) (e) SA- β-Gal assay of control (shLuc) and HIRA-deficient (sh1,2-HIRA) senescent cells. (f) EdU assay was performed by

treating cells with 10 μM EdU for 4 hours. (g) Real-time qPCR analysis showing the expression of SASP genes after 10 days of 20 Gy X-ray (h) IMR90 cells were infected with an inducible oncogenic ER:RAS construct using 4-hydroxy-tamoxifen (4-OHT). HIRA depletion was achieved in IMR90 ER:RAS cells using shRNAs. Real-time qPCR analysis showing the expression of SASP genes after seven days of 4-OHT treatment. (i) Immunoblot analysis of senescent cells treated with various doses of ML-792 drug for seven days. Immunoblot analysis of (j) UBC9-depleted senescent cells using UBE2I siRNA, (k) PML-depleted senescent cells using shRNA.

Figure S3: A similar number of differentially expressed genes (DEGs) were observed in both *Δ*HIRA and wild-type samples when comparing senescent cells to proliferating cells.
Basic statistics of RNA-seq differential analysis are shown. a) Number of significantly upregulated/downregulated genes in EV(Pro) vs *Δ*HIRA (Sen), EV(Pro) vs EV (Sen), and EV (Sen) vs *Δ*HIRA (Sen) comparisons, using an FDR cutoff of 0.05. b) MA plot depicting the three groups of comparisons.

Figure S4: HIRA and PML are not necessary for the regulation of certain effectors involved in SASP.
Immunoblot analysis was performed on whole-cell lysates of senescent cells depleted of HIRA and PML using siRNA. The same lysates were utilized in Figure 1 (f-g) and Figure 4 (a-b).

Figure S5: HIRA exhibits a physical interaction with the autophagy regulator p62.
(a) Representative image demonstrating the colocalization of p62 in CCF. (b, c) Knockdown of PML using shRNA followed by immunoblot analysis of p62 after HIRA pull-down. (d) Representative image displaying the efficiency of PML knockdown using siRNA. (e, f) Measurement of intensity and number of PML foci based on microscopic data to calculate the efficiency of PML siRNA.

References:

1. J. P. Coppe, P. Y. Desprez, A. Krtolica, J. Campisi, The senescence-associated secretory phenotype: the dark side of tumor suppression. *Annu Rev Pathol* **5**, 99-118 (2010).
2. D. McHugh, J. Gil, Senescence and aging: Causes, consequences, and therapeutic avenues. *J Cell Biol* **217**, 65-77 (2018).
3. C. Lopez-Otin, M. A. Blasco, L. Partridge, M. Serrano, G. Kroemer, Hallmarks of aging: An expanding universe. *Cell* **186**, 243-278 (2023).
4. C. D. Wiley, J. Campisi, The metabolic roots of senescence: mechanisms and opportunities for intervention. *Nat Metab* **3**, 1290-1301 (2021).
5. Y. Chien *et al.*, Control of the senescence-associated secretory phenotype by NF-kappaB promotes senescence and enhances chemosensitivity. *Genes Dev* **25**, 2125-2136 (2011).
6. X. Hao, C. Wang, R. Zhang, Chromatin basis of the senescence-associated secretory phenotype. *Trends Cell Biol* **32**, 513-526 (2022).
7. A. Takahashi *et al.*, Downregulation of cytoplasmic DNases is implicated in cytoplasmic DNA accumulation and SASP in senescent cells. *Nat Commun* **9**, 1249 (2018).
8. F. Rodier *et al.*, DNA-SCARS: distinct nuclear structures that sustain damage-induced senescence growth arrest and inflammatory cytokine secretion. *J Cell Sci* **124**, 68-81 (2011).
9. A. Ivanov *et al.*, Lysosome-mediated processing of chromatin in senescence. *J Cell Biol* **202**, 129-143 (2013).

10. Z. Dou *et al.*, Cytoplasmic chromatin triggers inflammation in senescence and cancer. *Nature* **550**, 402-406 (2017).
11. H. Yang, H. Wang, J. Ren, Q. Chen, Z. J. Chen, cGAS is essential for cellular senescence. *Proc Natl Acad Sci U S A* **114**, E4612-E4620 (2017).
12. S. Gluck *et al.*, Innate immune sensing of cytosolic chromatin fragments through cGAS promotes senescence. *Nat Cell Biol* **19**, 1061-1070 (2017).
13. T. S. Rai *et al.*, HIRA orchestrates a dynamic chromatin landscape in senescence and is required for suppression of neoplasia. *Genes Dev* **28**, 2712-2725 (2014).
14. A. D. Goldberg *et al.*, Distinct factors control histone variant H3.3 localization at specific genomic regions. *Cell* **140**, 678-691 (2010).
15. D. Filipescu, S. Muller, G. Almouzni, Histone H3 variants and their chaperones during development and disease: contributing to epigenetic control. *Annu Rev Cell Dev Biol* **30**, 615-646 (2014).
16. M. Narita *et al.*, Rb-mediated heterochromatin formation and silencing of E2F target genes during cellular senescence. *Cell* **113**, 703-716 (2003).
17. T. Chandra, Senescence associated heterochromatic foci: SAHF. *The Functional Nucleus*, 205-218 (2016).
18. R. Zhang *et al.*, Formation of MacroH2A-containing senescence-associated heterochromatin foci and senescence driven by ASF1a and HIRA. *Dev Cell* **8**, 19-30 (2005).
19. X. Ye *et al.*, Definition of pRB- and p53-dependent and -independent steps in HIRA/ASF1a-mediated formation of senescence-associated heterochromatin foci. *Mol Cell Biol* **27**, 2452-2465 (2007).
20. U. Sahin, H. de The, V. Lallemand-Breitenbach, PML nuclear bodies: assembly and oxidative stress-sensitive sumoylation. *Nucleus* **5**, 499-507 (2014).
21. A. M. Ishov *et al.*, PML is critical for ND10 formation and recruits the PML-interacting protein daxx to this nuclear structure when modified by SUMO-1. *J Cell Biol* **147**, 221-234 (1999).
22. S. F. Banani *et al.*, Compositional Control of Phase-Separated Cellular Bodies. *Cell* **166**, 651-663 (2016).
23. G. Ferbeyre *et al.*, PML is induced by oncogenic ras and promotes premature senescence. *Genes Dev* **14**, 2015-2027 (2000).
24. M. Vernier *et al.*, Regulation of E2Fs and senescence by PML nuclear bodies. *Genes Dev* **25**, 41-50 (2011).
25. O. Vladimirova *et al.*, Phase separation and DAXX redistribution contribute to LANA nuclear body and KSHV genome dynamics during latency and reactivation. *PLoS Pathog* **17**, e1009231 (2021).
26. J. S. Pawlikowski *et al.*, Wnt signaling potentiates nevogenesis. *Proc Natl Acad Sci U S A* **110**, 16009-16014 (2013).
27. S. Hirano, O. Udagawa, Effects of arsenic on the topology and solubility of promyelocytic leukemia (PML)-nuclear bodies. *PLoS One* **17**, e0268835 (2022).
28. N. Basisty *et al.*, A proteomic atlas of senescence-associated secretomes for aging biomarker development. *PLoS Biol* **18**, e3000599 (2020).
29. L. Zhang, L. E. Pitcher, V. Prahalad, L. J. Niedernhofer, P. D. Robbins, Targeting cellular senescence with senotherapeutics: senolytics and senomorphics. *FEBS J* **290**, 1362-1383 (2023).
30. M. Chen *et al.*, TRIM14 Inhibits cGAS Degradation Mediated by Selective Autophagy Receptor p62 to Promote Innate Immune Responses. *Mol Cell* **64**, 105-119 (2016).

31. R. D. Everett, M. K. Chelbi-Alix, PML and PML nuclear bodies: implications in antiviral defence. *Biochimie* **89**, 819-830 (2007).
32. A. Ablasser, Z. J. Chen, cGAS in action: Expanding roles in immunity and inflammation. *Science* **363**, (2019).
33. T. S. Rai *et al.*, Histone chaperone HIRA deposits histone H3.3 onto foreign viral DNA and contributes to anti-viral intrinsic immunity. *Nucleic Acids Res* **45**, 11673-11683 (2017).
34. S. McFarlane *et al.*, The histone chaperone HIRA promotes the induction of host innate immune defences in response to HSV-1 infection. *PLoS Pathog* **15**, e1007667 (2019).
35. V. Lallemand-Breitenbach, H. de The, PML nuclear bodies. *Cold Spring Harb Perspect Biol* **2**, a000661 (2010).
36. S. Zhong *et al.*, Role of SUMO-1-modified PML in nuclear body formation. *Blood* **95**, 2748-2752 (2000).
37. A. M. Andreou, N. Tavernarakis, Roles for SUMO modification during senescence. *Adv Exp Med Biol* **694**, 160-171 (2010).
38. L. Ivanschitz, H. De The, M. Le Bras, PML, SUMOylation, and Senescence. *Front Oncol* **3**, 171 (2013).
39. C. Kang *et al.*, The DNA damage response induces inflammation and senescence by inhibiting autophagy of GATA4. *Science* **349**, aaa5612 (2015).
40. K. K. Jena *et al.*, Autoimmunity gene IRGM suppresses cGAS-STING and RIG-I-MAVS signaling to control interferon response. *EMBO Rep* **21**, e50051 (2020).
41. T. Prabakaran *et al.*, Attenuation of cGAS-STING signaling is mediated by a p62/SQSTM1-dependent autophagy pathway activated by TBK1. *EMBO J* **37**, (2018).
42. W. Xie *et al.*, OTUD7B deubiquitinates SQSTM1/p62 and promotes IRF3 degradation to regulate antiviral immunity. *Autophagy* **18**, 2288-2302 (2022).
43. M. D. Ricketts *et al.*, The HIRA histone chaperone complex subunit UBN1 harbors H3/H4 and DNA binding activity. *J Biol Chem*, (2019).
44. F. Debacq-Chainiaux, J. D. Erusalimsky, J. Campisi, O. Toussaint, Protocols to detect senescence-associated beta-galactosidase (SA-betagal) activity, a biomarker of senescent cells in culture and in vivo. *Nat Protoc* **4**, 1798-1806 (2009).
45. A. Salic, T. J. Mitchison, A chemical method for fast and sensitive detection of DNA synthesis in vivo. *Proc Natl Acad Sci U S A* **105**, 2415-2420 (2008).
46. M. G. Vizioli *et al.*, Mitochondria-to-nucleus retrograde signaling drives formation of cytoplasmic chromatin and inflammation in senescence. *Genes Dev* **34**, 428-445 (2020).
47. A. Dobin *et al.*, STAR: ultrafast universal RNA-seq aligner. *Bioinformatics* **29**, 15-21 (2013).
48. P. Danecek *et al.*, Twelve years of SAMtools and BCFtools. *Gigascience* **10**, (2021).
49. C. Trapnell *et al.*, Transcript assembly and quantification by RNA-Seq reveals unannotated transcripts and isoform switching during cell differentiation. *Nat Biotechnol* **28**, 511-515 (2010).
50. F. Ramirez *et al.*, deepTools2: a next generation web server for deep-sequencing data analysis. *Nucleic Acids Res* **44**, W160-165 (2016).
51. G. H. Putri, S. Anders, P. T. Pyl, J. E. Pimanda, F. Zanini, Analysing high-throughput sequencing data in Python with HTSeq 2.0. *Bioinformatics* **38**, 2943-2945 (2022).
52. M. I. Love, W. Huber, S. Anders, Moderated estimation of fold change and dispersion for RNA-seq data with DESeq2. *Genome Biol* **15**, 550 (2014).

Figure 1 : HIRA and PML are required for SASP expression but not for proliferation arrest.

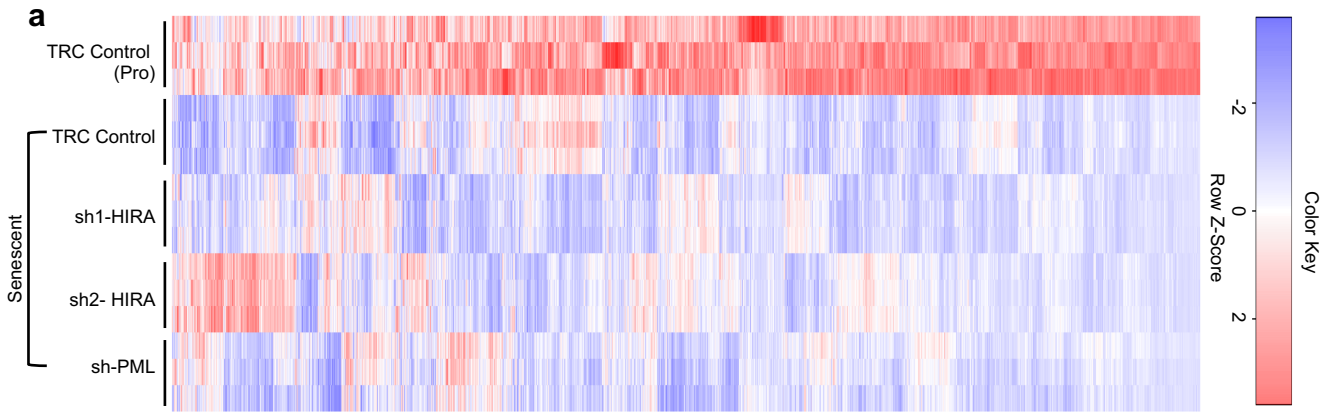

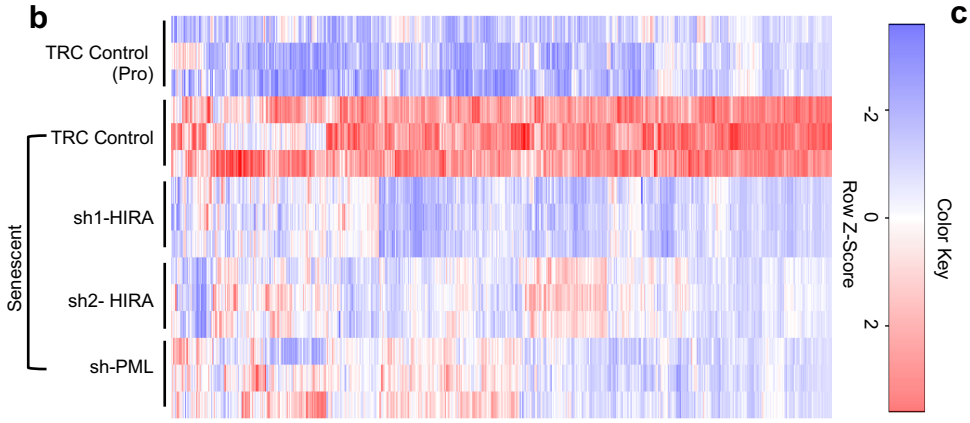

c

Top Upstream Regulators	p-values
TNF	$8.45X10^{-28}$
IL1B	$1.63X10^{-25}$
Lipopolysaccharide	$1.96X10^{-24}$
NFκB (Complex)	$1.04X10^{-21}$
IFNG	$6.39X10^{-21}$
Poly rI:rC-RNA	$7.17X10^{-21}$

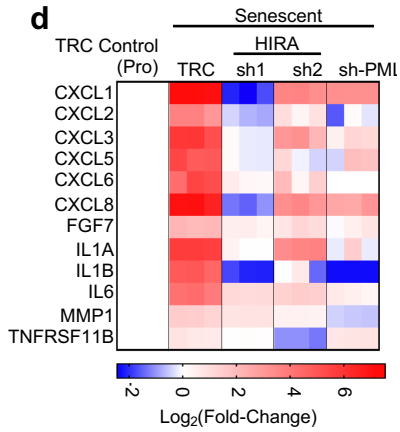

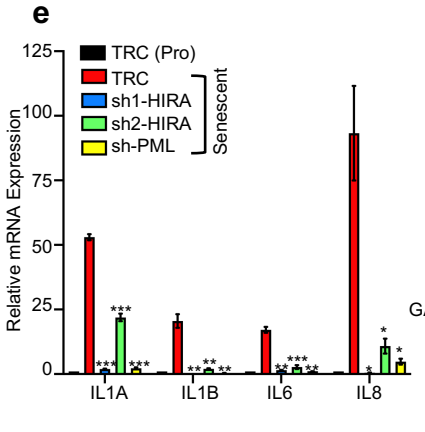

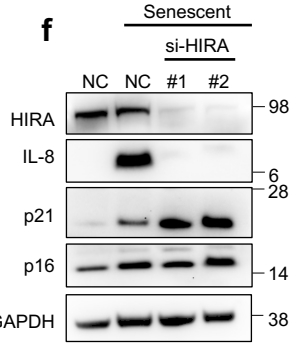

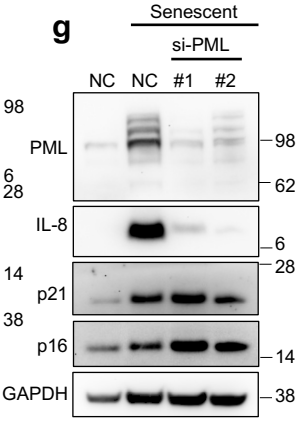

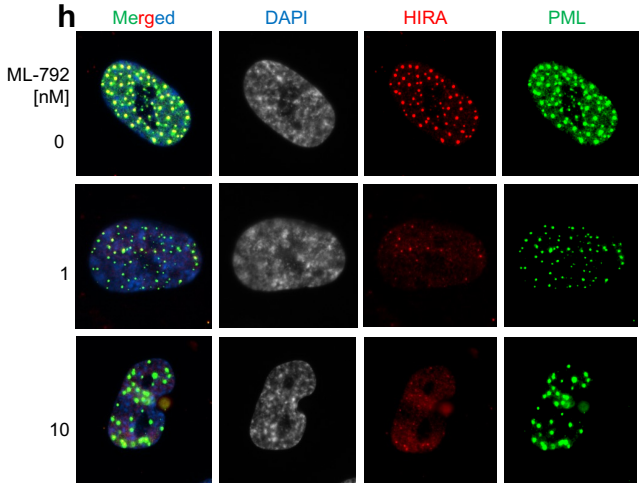

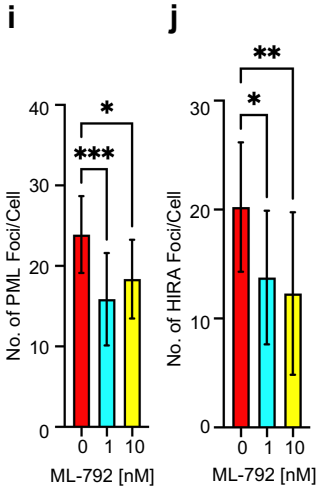

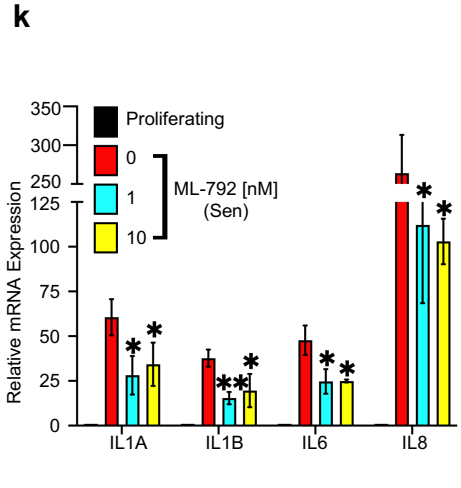

Figure 2 : Localization of HIRA in PML bodies is tightly linked SASP expression.

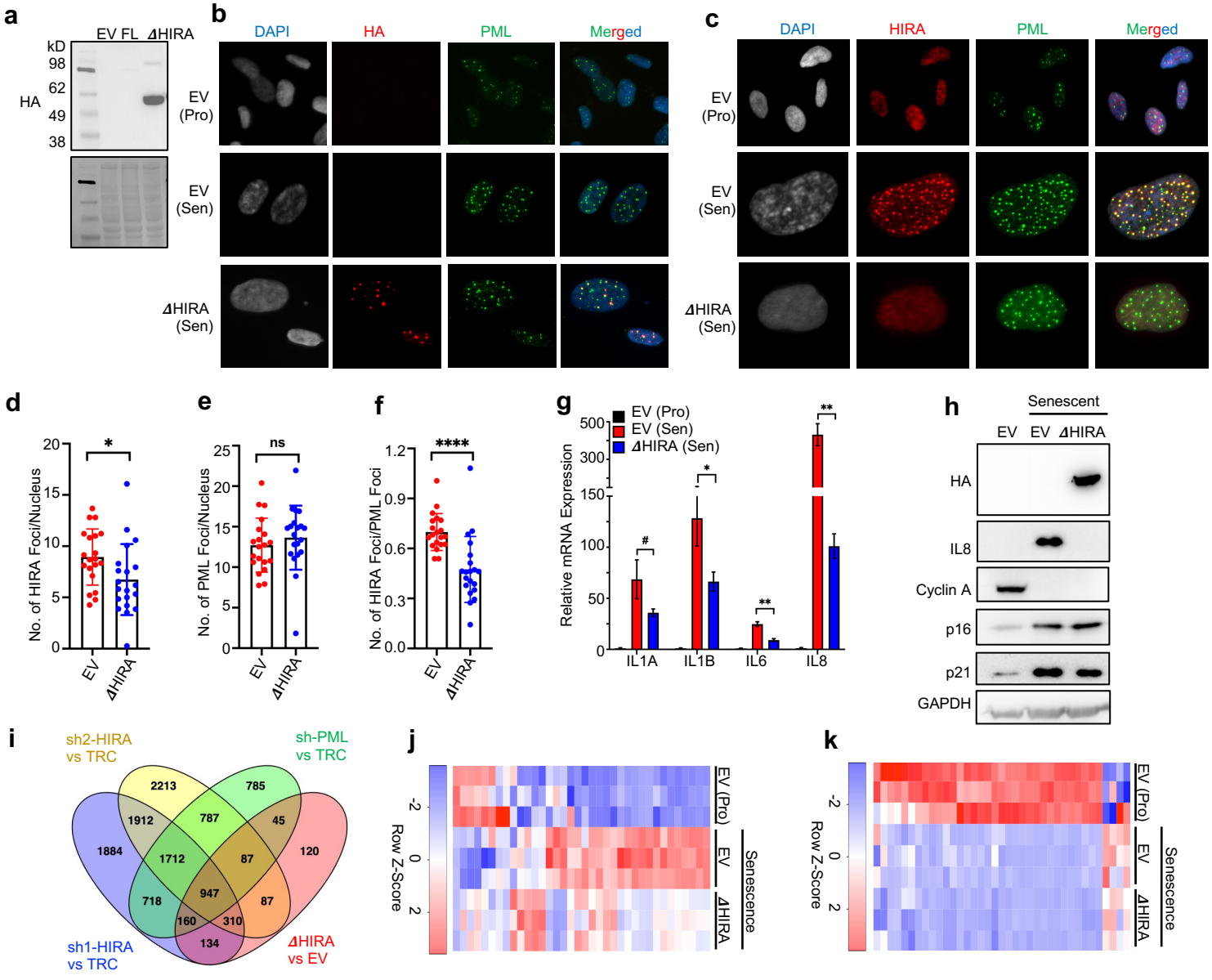

Figure 3: HIRA regulates SASP through activation of NF-κB pathway independent of it's H3.3 deposition role

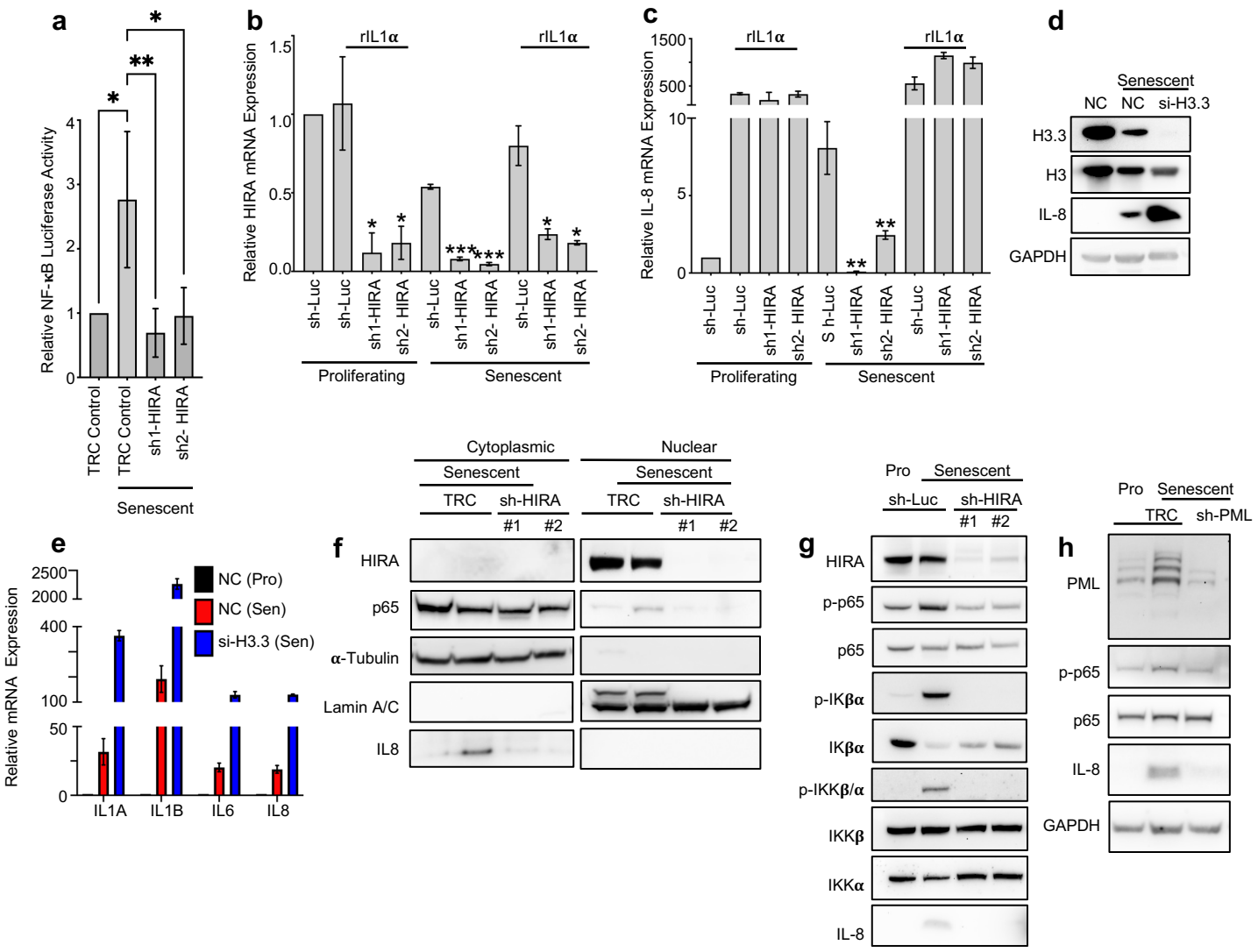

Figure 4: HIRA and PML are required for cGAS-STING-TBK1 signalling.

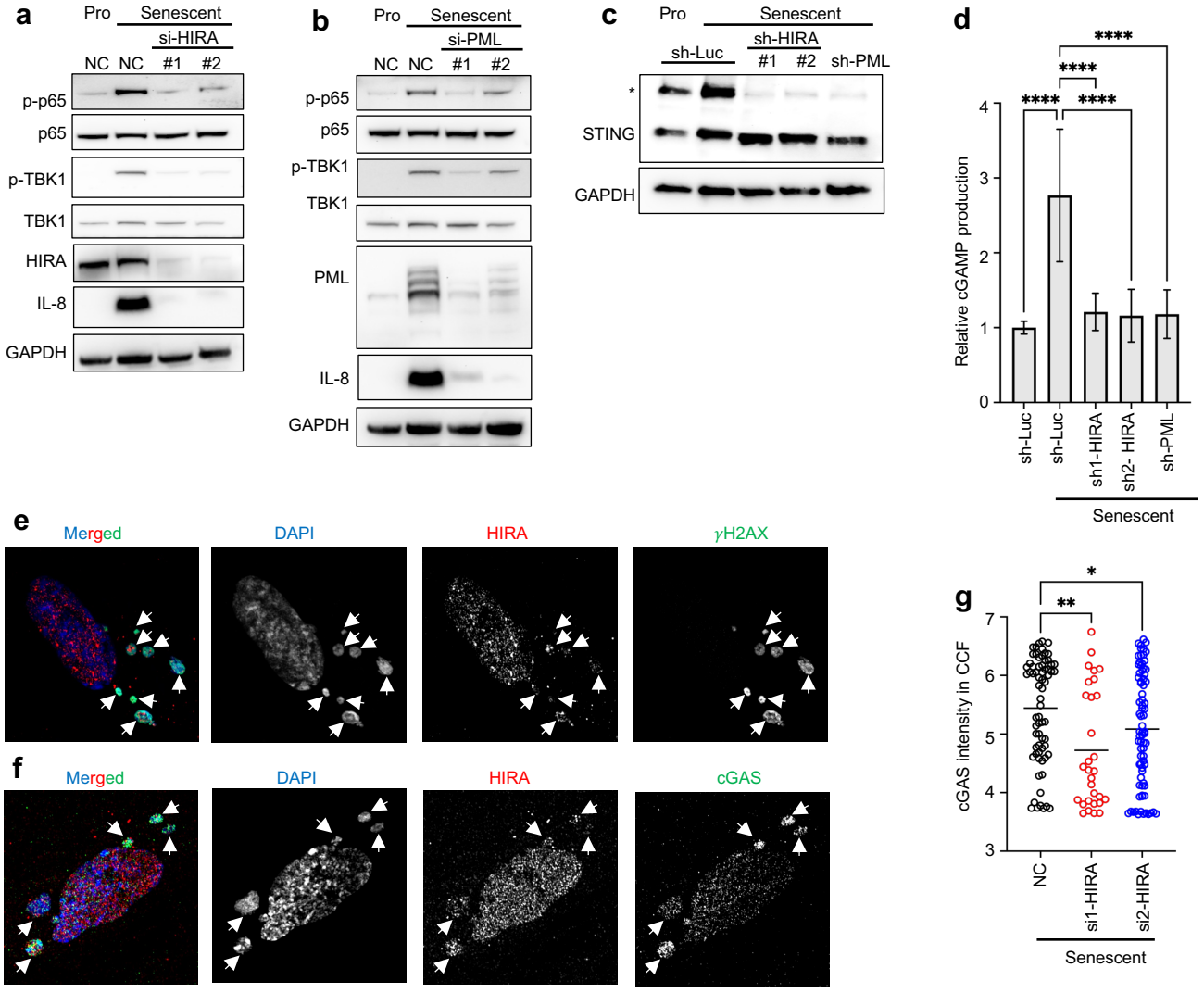

Figure 5: HIRA physically interacts with autophagy regulator p62 to regulate SASP expression.